

Calcitic Prisms of The Giant Seashell *Pinna Nobilis* Form Light Guide Arrays

Shahrouz Amini,* Tingting Zhu, Abin Biswas, Mohammad Avalin Charsooghi, Kyoohyun Kim, Simone Reber, Yannicke Dauphin, and Peter Fratzl*

The shells of the *Pinnidae* family are based on a double layer of single-crystal-like calcitic prisms and inner aragonitic nacre, a structure known for its outstanding mechanical performance. However, on the posterior side, shells are missing the nacreous layer, which raises the question of whether there can be any functional role in giving up this mechanical performance. Here, it is demonstrated that the prismatic part of the *Pinna nobilis* shell exhibits unusual optical properties, whereby each prism acts as an individual optical fiber guiding the ambient light to the inner shell cavity by total internal reflection. This pixelated light channeling enhances both spatial resolution and contrast while reducing angular blurring, an apt combination for acute tracking of a moving object. These findings offer insights into the evolutionary aspects of light-sensing and imaging and demonstrate how an architected optical system for efficient light-tracking can be based on birefringent ceramics.

structural complexity arose from coexistence and/or local alteration^[2] of the deployed microarchitectures such as cross-lamellar, prismatic, foliated, and nacreous, and introduced inter-crystalline and intra-crystalline interfaces are explained as factors serving the mechanical function of the shells. Among these, the nacreous architecture got the greatest attention thanks to its promising fracture toughness.^[3] Notably, in the *Pinnidae* family, despite the bivalves' capability to form the nacreous layer,^[4] the posterior side of the shells is solely formed of a prismatic layer.^[5] Here, we are reporting an unexpected observation that shows the prismatic layer of the *P. nobilis* shell transmits the environmental light and projects shadows of external objects to the inner part of the shells, integrating a remarkable

optical system into the mineralized armor of the animal. We hypothesize that this optical characteristic may be associated with the photobiological behavior of the animal, such as known shell gapping reactions to changes in environmental light intensity^[6] and the shell's closure reaction to approaching shadow.^[6a,d] Accordingly, we designed and conducted a series of optical experiments to understand the light-shell interactions in different length scales ranging from single prism to full-scale shell.

1. Introduction


The microarchitectural organization presented in mineralized shells of mollusks is mainly attributed to the primary function of "protection against external threats".^[1] Accordingly, the

S. Amini, T. Zhu, M. A. Charsooghi, P. Fratzl
Max Planck Institute of Colloids and Interfaces
Department of Biomaterials
14476 Potsdam, Germany
E-mail: Shahrouz.Amini@mpikg.mpg.de; Peter.Fratzl@mpikg.mpg.de

A. Biswas, S. Reber
Max Planck Institute for Infection Biology
10117 Berlin, Germany

A. Biswas, K. Kim
Max Planck Institute for the Science of Light
91058 Erlangen, Germany

Y. Dauphin
UMR 7205 ISYEB
Museum National d'histoire Naturelle
CNRS UPMC EPHE
57 rue Cuvier, Paris 75005, France

 The ORCID identification number(s) for the author(s) of this article can be found under <https://doi.org/10.1002/adma.202304166>

© 2023 The Authors. Advanced Materials published by Wiley-VCH GmbH. This is an open access article under the terms of the Creative Commons Attribution License, which permits use, distribution and reproduction in any medium, provided the original work is properly cited.

DOI: 10.1002/adma.202304166

2. Results and Discussion

2.1. Translucency

P. nobilis – noble pen shells or fan mussels – are shallow water mollusks well-studied for the uncommon geometrical and structural features of their shells,^[5a] which can grow up to 120 cm.^[7] Unlike many other bivalves, *P. nobilis* often stands in a vertical position (Figure 1a; Figure S1, Supporting Information), inserting the tapered anterior ends of the shells in the seabed and anchoring them with the strong byssus threads.^[6d,8] While the tapered anterior end of the shell is nacreous – prismatic bi-layered,^[5a] the posterior side is solely formed by single-crystal-like prismatic calcite (Figure 1b). The presence of prismatic structure as a dominant fraction of the seashell surface without the second layer is extremely rare, and the presence of single-crystal-like prisms extending from the shells' outer surface to the inner cavity is only limited *P. nobilis* and *Atrina* (*Pterioide* bivalves).^[9]

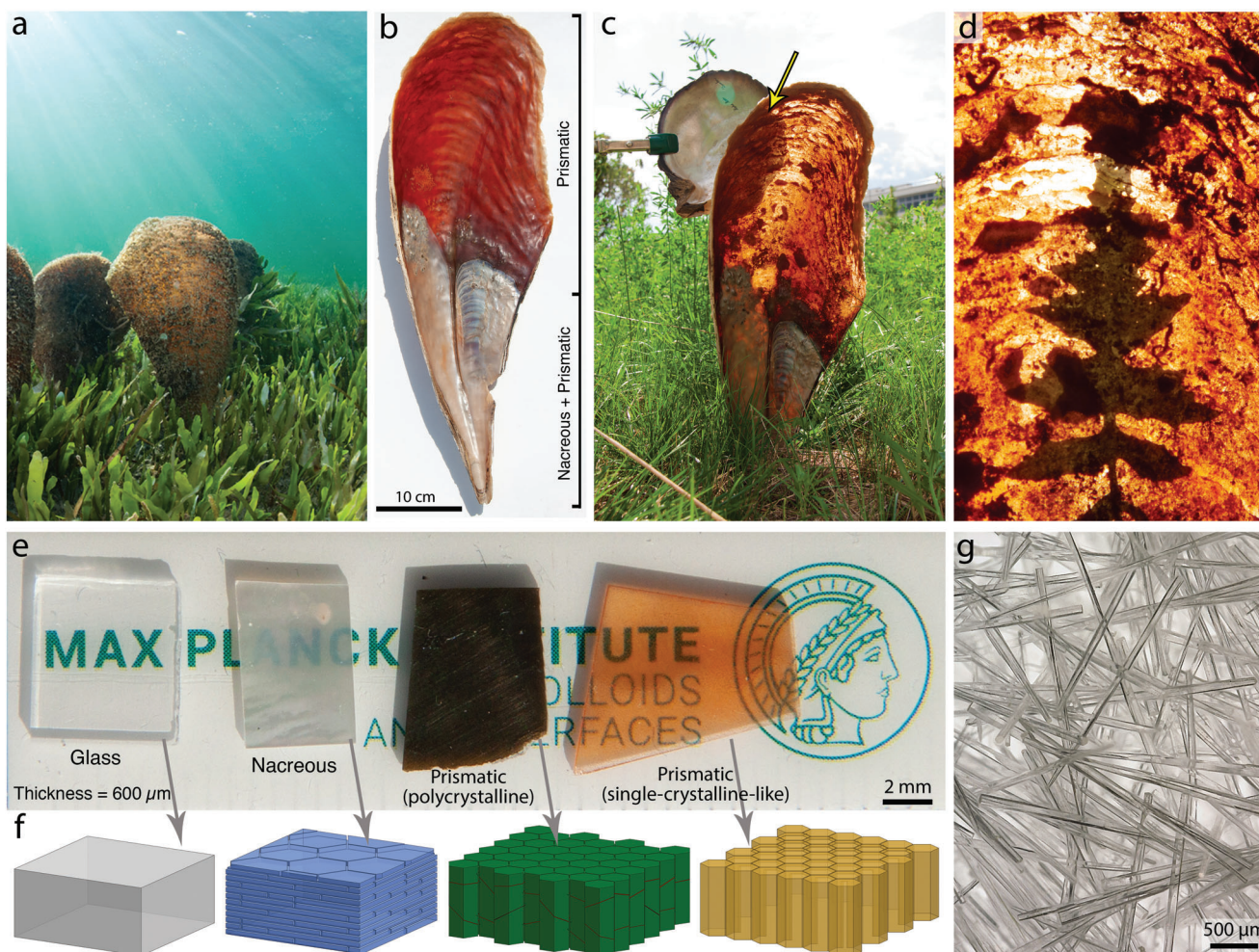


Figure 1. Optical transparency of *P. nobilis* shells. a) *P. nobilis* in its habitat (Mar Menor lagoon, Spain) Credit: Javier M-urcia. b) Photograph of the inner side of a *P. nobilis* shell revealing the absence of the nacreous layer at the posterior part of the shell. c) Advances of the light through the entire posterior part of *P. nobilis* shell projecting the shadow of surrounding objects on the inner wall of the shell. In contrast, the *Pinctada* shell could totally block the sunlight (Figure S1, Video S1, Supporting Information). d) Photograph highlighting the projected shadow of a leaf with its clear margins on the internal wall of a *P. nobilis* shell. e) Photograph of individual shell slices ($t = 600 \mu\text{m}$) compared to a glass slide placed on the MPICI institution logo without exposure to any backlight. f) Schematic illustration of the corresponding microarchitectural organization of the individual slices (see panel e). g) Single-crystal-like prisms of *P. nobilis* shell after treatment by bleaching agent and removing their organic envelope.

In mature *P. nobilis*, the prisms can reach up to 3 mm (Figure 1g), extending from the shells' outer surface to the inner cavity. Surprisingly, despite the shell thickness (prism length), light can advance through the entire prismatic shell and project the shadows of surrounding objects on the inner wall of the shells (Figure 1c,d, Video S1, Supporting Information). Considering the habitat of *P. nobilis* – shallow water zones of tropical and subtropical seas – the animals in their native condition are exposed to environmental light, and their gapping behavior is sensitive to light intensity.^[6b–d] Hence, the interaction with environmental light/shadow, even under full moonlight,^[6b,c] is considered to contribute to the biologically relevant function of the animals, such as circadian and circalunar rhythms.^[6d]

Transparency in seashells has been studied in foliated shells of *Placuna placenta*.^[10] However, to the best of our knowledge, the transparency in prismatic shells has been noticed^[11] but has not been studied. Accordingly, *Pinctada margaritifera*, a nacro-

prismatic model connected to *P. nobilis* from a taxonomical point of view, was selected as a comparative model. However, unlike *P. nobilis*, the outer prismatic layer in the *Pinctada* shell is almost entirely underlaid with a nacreous layer. Notably, by exposing the *Pinctada* shells to ambient light, we noticed that the shell could block it. This was also true when the shell was exposed directly to sunlight (Figure 1c; Figure S2, Supporting Information).

To understand the light interaction with the individual shell layers and their microarchitectural organizations, we isolated individual shell layers by sectioning and polishing them to form slices with the same thickness ($t = 600 \mu\text{m}$) and compared them with a glass slide as a transparent reference. Figure 1e shows that besides glass, the light transmission through the *P. nobilis* shell slice allowed a clear vision of the text with no distortion or double refraction. We attributed this clarity to the preferred orientation of the calcitic prisms of *P. nobilis* along their *c*-axis^[5a] – equal to the ordinary optical axis of calcite – minimizing, if not

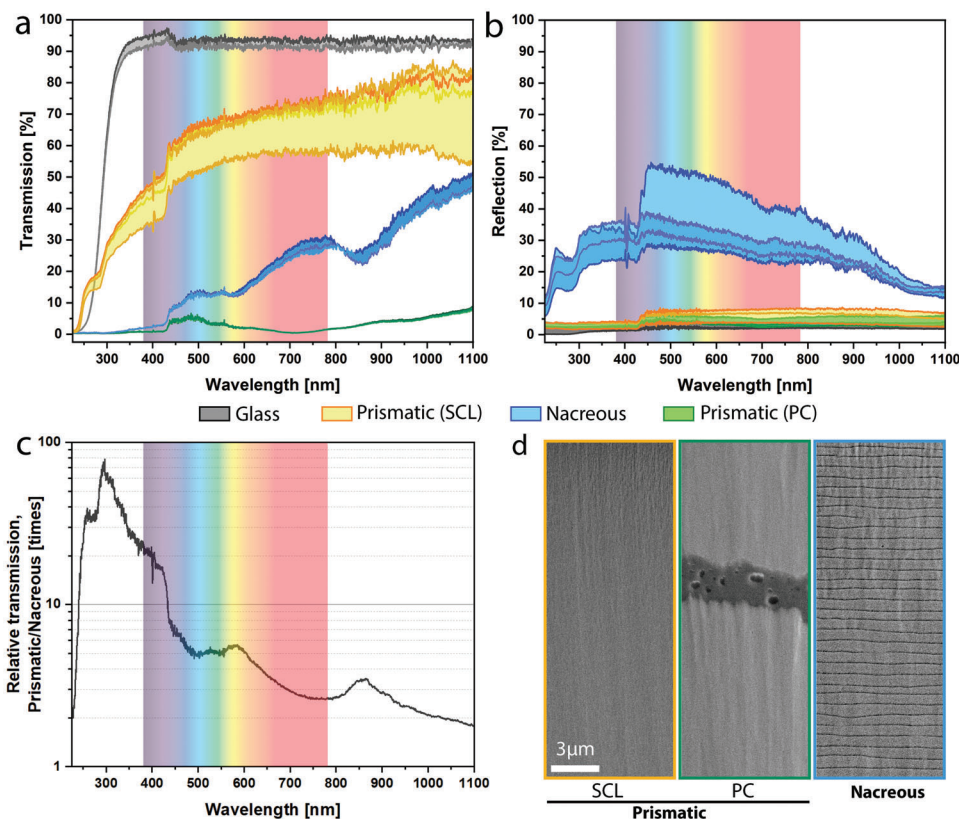


Figure 2. Optical characteristics of individual prismatic and nacreous layers. a) Light transmission of *P. nobilis* prismatic shell slice ($t = 0.6$ mm, depicted in orange) compared with a glass (in grey) and *Pinctada* prismatic shell slice (in green), denoting the high translucency of the *P. nobilis* prismatic shell. b) High reflectivity of the nacreous architecture matches the layer's inability to transmit incident lights. c) Relative light transmission of prismatic and nacreous layers presenting 2 to 80 times higher light transmission in the prismatic layer of *P. nobilis*. d) Scanning electron micrographs from an ion-sectioned transversal plane of the shells illustrating the absence of the organic interfaces in the single-crystal-like prism of *P. nobilis* (SCL). In contrast, the polycrystalline prism (PC) and the nacreous layer of *Pinctada* possess thick and repetitive organic interfaces, respectively. The panels share the same scale bar.

avoiding, light transmission along the extraordinary axis of calcite and canceling the double refraction.^[12] Besides, the single-crystal-like structure of the *P. nobilis* prisms and their extension all along the shell wall result in the absence of interfacial reflection and scattering.^[12] In stark contrast, the prismatic slice of the *Pinctada* shells – known for their polycrystalline structure with their *c*-axis perpendicular to the long morphological axis of the prism^[13] – prevented any light transmission. The nacreous slice showed a better light transmission, yet it barely allowed detection of the text.

To quantify light interactions, we measured the relative transmission and reflection of the slides by exposing them to a light source with a broad spectral coverage (250–1100 nm). The collected spectra revealed that the *P. nobilis* slice transmitted the main fraction of the incident visible light (50–70%), while in *Pinctada*, the polycrystalline^[14] prisms and the nacreous layer only transmitted a minor fraction (10–30% and less than 5%, respectively) (Figure 2a). Notably, the light transmission in the *P. nobilis* shell was not limited to the visible range and included 15–45% transmission in the UV range. In sharp contrast, the nacreous structure acted as a mirror, reflecting 20–50% of the incident light, including UV (Figure 2b). This mirror-like behavior can be attributed to the architectural organization of the

nacreous layer^[15] and the thickness distribution of the platelets (400–750 nm), which stays in the ambient light wavelength range (Figure 2d-right panel and Figure S3, Supporting Information). A quantitative comparative analysis was made by plotting the relative light transmission of the prismatic and nacreous samples revealing a 2 to 80 times higher light transmission in the prismatic layer of the *P. nobilis* shell (Figure 2c). Finally, the low (<5%) reflectivity of the polycrystalline prisms along with the low (<5%) transmission indicated that the main fraction of the incident light to this layer was absorbed or internally scattered. It is worth mentioning that in aquatic environments, the component wavelengths of sunlight are differently absorbed by the water column.^[16] However, the inhabitant of *P. nobilis* stays within the very upper range of the euphotic zone,^[17] in which light wavelengths are absorbed fairly uniformly.

2.2. Containment and Channeling of Light by Total Internal Reflection

To uncover the light transmission mechanism of the single-crystal-like prisms ($d = 50$ – 100 μm), we examined *P. nobilis* shell slices ($t = 1$ mm) by exposing them to a narrow beam with a

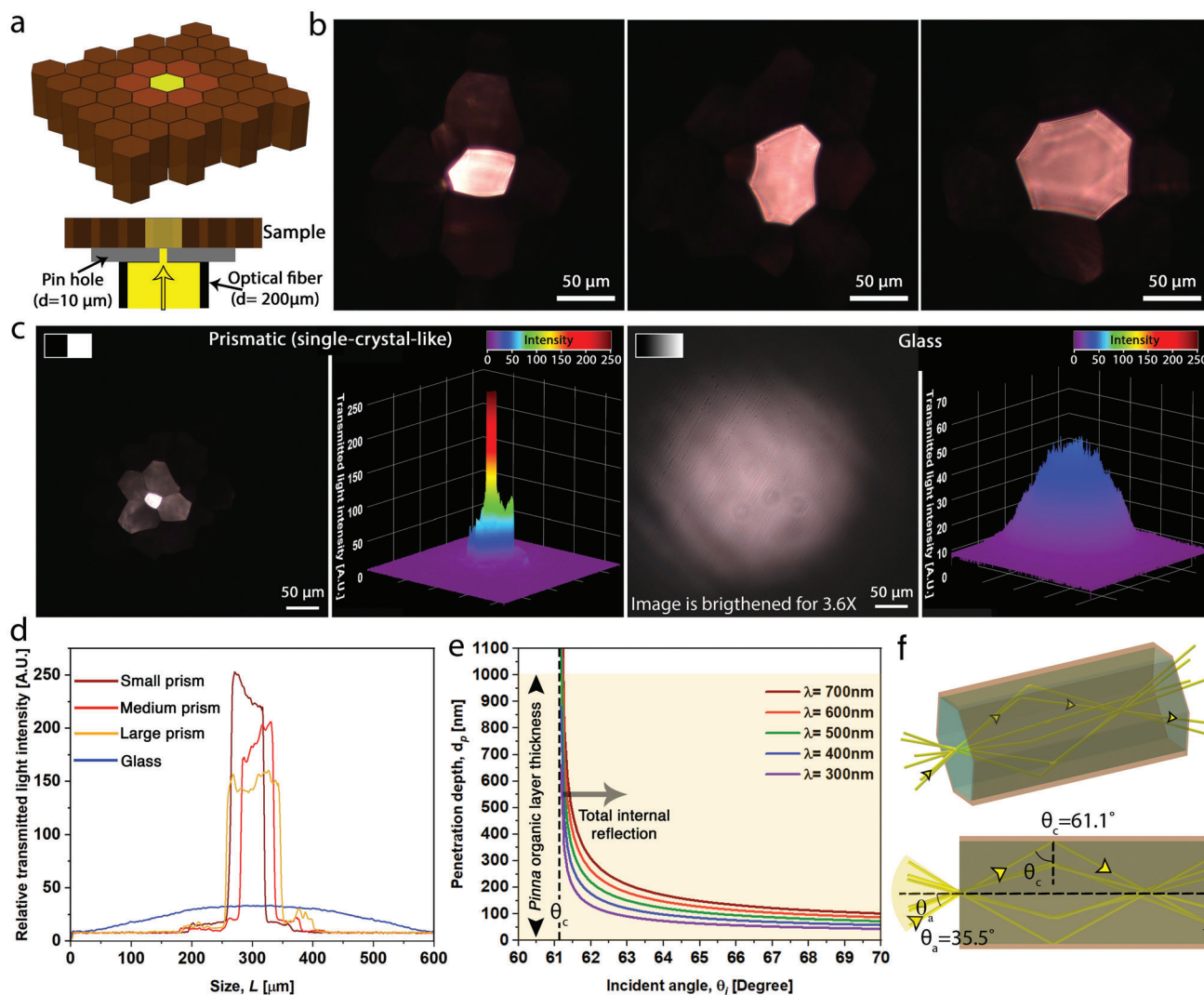


Figure 3. Total internal refraction results in guided transmission of light. a) Schematic image of the setup used for intra-prismatic light transmission studies. b) Transmitted light through the prisms directly exposed to a 10 μm pinhole revealing that light can be contained within the prisms. c) Comparative illustration of the transmitted light profile from the calcitic prism (left panels) and a glass slide (right panels). While the volume of the transmitted light (measured by volume integration of the light profiles) through the glass is higher, the localized intensity of light in the prism is about fivefold higher. d) Comparative illustration of 2D intensity plots of the transmitted lights in prisms with the different cross-sectional areas and a glass slide. e) Calculated penetration depth of evanescent wave for different wavelengths showing that the incident lights to the inner walls of the prisms can barely pass the thick organic envelope ($t = 1 \mu\text{m}$), avoiding the inter-prismatic cross talks. The dashed line represents the critical angle. f) Schematic image illustrating the light rays – *P. nobilis* prism interactions and calculated acceptance angle (θ_a) and critical angle (θ_c) in a seawater environment ($RI = 1.34$).

spot size of 10 μm (see Experimental Section), ensuring that the light can only enter one prism (Figure 3a). The observed transmitted light spot with minimal or zero light leakage to the neighboring prisms revealed that each prism could remarkably contain the incident light and guide it across the slice. By moving the light beam along the slice, we noticed that despite the constant intensity of the incident light, the transmitted light intensity varies inversely with prism width (Figure 3a,b,d): the transmitted light from a smaller prism showed a higher intensity. Moreover, by comparing the light profiles transmitted from *P. nobilis* shell and glass slices ($t = 1 \text{ mm}$), we found that despite a higher light transmission in glass, as evidenced by volume integration of the light profiles, prisms could avoid light divergence, resulting

in a concentrated light spot with about fivefold intensity higher than the transmitted light from the glass slide. In addition, we realized that the intensity of the transmitted light has a homogeneous distribution across the prisms section, contrasting with Gaussian light distribution that develops in non-architected and homogenous media such as air and glass. Yet, in some cases, this homogeneity in transmitted light intensity experienced an interference pattern (Figure 3b; Figure S4a, Supporting Information), denoting the formation of phase shifts known to be induced by internal refraction inside the prisms.^[12] These observations suggested that the transmission of the light inside the single-crystal-like prisms occurs through a total internal reflection phenomenon.

To better understand the principle of the light interactions within individual prisms and quantify the optical parameters of the *P. nobilis* shell, we used optical diffraction tomography (ODT), a holographic microscopy technique, to quantitatively measure the 3D refractive index (RI) distribution of prism and organic shield (See Experimental Section) individually.^[18] As expected, due to the preferred orientation of the calcitic prisms along their *c*-axis (ordinary optical axis), a high RI of 1.61 ($n = 10$, individual prisms) was measured for the calcitic prisms (Figure S5, Supporting Information). This value was slightly lower than the reported value for the RI of geological calcite along their optical axis ($RI_{or} = 1.66$). This difference can be attributed to the presence of organic residues in the biological calcite.^[19] The measured RI value of the organic shield ($RI = 1.41$, $n = 10$, individual pieces of organic shields) and the proximity to the RI of calcite along the extraordinary axis ($RI_{ex} = 1.49$) revealed how a preferred alignment along the ordinary optical axis (*c*-axis) of the prisms can be beneficial for decreasing the total internal reflection angle. We found that by alignment of the calcitic prisms along their *c*-axis, the critical angle (θ_c) – the angle of incidence above which total internal reflection occurs – of the prisms in seawater ($RI = 1.34$ ^[20]) decreased by 14% (71.1° in the extraordinary optical axis of calcite vs 61.1° in *P. nobilis*), resulting in a 68% increment (21.1° in the extraordinary optical axis of calcite vs 35.5° in *P. nobilis*) in the acceptance angle (θ_a) – the maximum angle at which incident light can be captured by the prisms – (Figure 3f). Remarkably, the enhancement in acceptance angle and numerical aperture resulted in a 2.75-fold increment in light-gathering power (See Experimental Section). In other words, the alignment of the prisms along their *c*-axis can increase the oblique angles to collect a larger quantity of ambient light, enhancing the light sensitivity of the prismatic shells, critical criteria for light interacting models in aquatic environments.^[21] It has been reported that the animal can react to sudden darkness even at night under full moonlight^[6b,c] implying the high responsiveness of the animal even under low light conditions. This behavior can explain the need for high light-gathering power.

In addition, the calculated penetration depth of evanescent waves^[12] – propagated light due to the total internal reflection – for different wavelengths of the incident light (Figure 3e) revealed the importance of a thick (1–2 μm) organic envelope in preventing light leakage to the neighbor prisms. Nevertheless, in some cases, we could detect light leakages to the neighbor prisms (Figure 3c-left panel and Figure S4b, Supporting Information). We suggest that the size and taper angle of the shrinking or growing prisms^[22] may violate the critical incident angle and contribute to the leakage (if any) of the contained light to the neighbor prisms.

Besides, by growing the prisms across the shell thickness, some prisms shrink and get eliminated,^[22] resulting in localized blockage of the light and deterioration of the transmitted shadow. Yet, considering the density of the prisms (≈ 500 prisms per inch, ppi), the prism elimination effect at its natural occurrence does not affect the reported optical characteristics.

Later, we designed an experiment to evaluate the performance of an individual – isolated – calcitic prism (with a prism length $l = 1.8$ mm) by exposing it to a light beam (with optical fiber diameter $d = 200$ μm) at different incident angles (Figure 4a, see Experimental Section). In good agreement with our previous obser-

vations, the transmitted light at the free end of the prism showed a bright glow (Figure 4a, blue arrowhead), closely resembling the function of an optical fiber/ light guide. Our observations showed that despite the changes in the intensity of the transmitted light, by changing the incident angle, the light can be fairly transmitted through the individual prism.

2.3. Enhancement in Spatial Resolution and Contrast

Because of the displayed optical characteristics and geometrical features of the individual calcitic prisms of *P. nobilis*, we compared them with the apposition compound eye's crystalline cones,^[16,23] in which cones act as optically isolated light guides guiding the light by total internal reflection^[23a,24] or mirroring effect in the crystalline cone of decapod crustacean eyes.^[25] In these optical systems, the physical characteristics of the cone bundles define the resolution of the spatial information which can be transferred to the compound eye. Accordingly, to examine the optical performance of the calcitic prisms and evaluate the interrelationships between the microarchitectural organization of the prisms and induced spatial resolution, we designed two experiments in reflection and transmission modes.

By probing *P. nobilis* shells with a reflected light microscope and changing the light spot size with the microscope aperture, we noticed that the shaped light spot on the shell did not match the hexagonal geometry of the aperture (Figure 4b, dotted hexagons). Instead, the light spot was defined by the basal size and arrangement of the illuminated prisms (Figure 4b), such that even by exposure of a small fraction of one prism, the entire prism was uniformly illuminated and outlined a new perimetric border. This denoted that each calcitic prism acts as a binary pixel that, upon the exposure or closure of the light, can be switched On or Off. Hence, by changing the light spot size, resembling a moving object, the perimetric prisms present a clear and acute track of light development, and the prismatic array can convey the spatial information of the incident light with resolution down to tens of micrometers, which is the basal size of the prisms (Figure 4b, Video S2, Supporting Information).

We then investigated the role of prismatic architecture and induced spatial resolution in tracking a moving object using transmitted light and whether this feature can be preserved across a native *P. nobilis* shell. Accordingly, we exposed a native *P. nobilis* shell ($t \approx 2$ mm) to a light beam (laser diode, $\lambda = 650$ nm) while moving the beam along the sample surface (Figure 4c, upper row). A glass slide ($t = 1$ mm), representing a translucent plain sample, was selected as a comparative reference (Figure 4c, lower row).

The pattern of the illuminated prisms indicated that by sweeping the light source along the shell surface, *P. nobilis* prisms could form a binary (On–Off/ Light–Shadow) illumination (Figure 4c, upper row, and Video S3, Supporting Information), which retains and transfers the spatial resolution and contrast of the external light/shadow spot to the inner surface of the prismatic shell. The exhibited resolution and contrast can potentially provide the required information for acute positioning and estimating the speed of a moving object's shadow (Figure 4d-upper panel, Note S1, Supporting Information). These outstanding features cannot be attained by homogenous media independent of material type

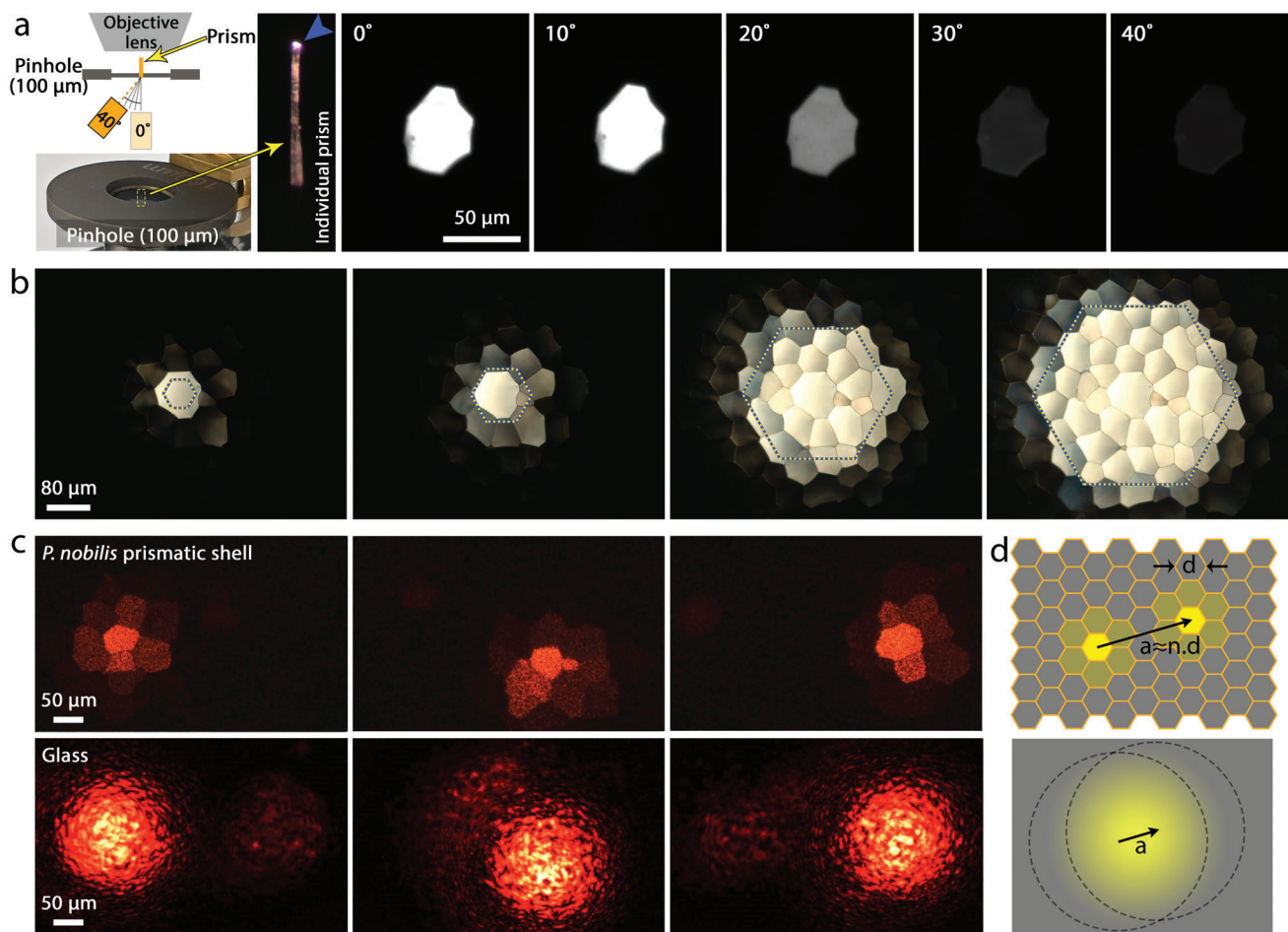


Figure 4. Pixelated containment of light within *P. nobilis*'s prisms. a) Guided light through an individual *P. nobilis* prism ($l \approx 1.8$ mm) in different angular exposure resembling an optical fiber. b) Reflected light spots on the *P. nobilis* slice revealing the mismatches between the peripheral edge of the illuminated prisms and the hexagonal geometry of the light spot formed by the microscope aperture denoted by the dashed hexagons. The macroscale mismatches induced by channeling the light within the calcitic prisms provide an accurate fit between the projected and transmitted light/shadow in the macroscale (Figure 1d,e; Figure S2, Supporting Information, middle row). c) Transmitted light spots formed by sweeping a light beam along a native prismatic *P. nobilis* shell (upper row) and a glass slide (bottom row), revealing the spatial resolution and contrast in the prismatic *P. nobilis* shell compared to the glass sample (see Video S3, Supporting Information). This characteristic, formed by the total internal reflection of the light in the calcitic prisms, introduces the prismatic *P. nobilis* shell as an optical light guide array for high-precision light/shadow tracking of a moving object. d) Schematic illustration presenting how pixelated light can foster spatial resolution for tracking a moving object.

(Figure 4d-lower panel). Figure 4d schematically illustrates how the tracking precision can be enhanced using a basic binary (On–Off/ Light–Shadow) illumination formed by the prismatic shell of *P. nobilis*.

2.4. Reduction in Sensitivity to Angular Exposure

We extended our investigations on the role of the prismatic array and induced pixelated light channeling on the formation of reflected and transmitted lights/shadows by designing and conducting an experiment on a replicated model. Accordingly, a frosted acrylic plate ($t = 3.2$ mm) was laser cut (see Experimental Section) to form an array of hexagonal prisms (Figure 5). By exposing the architected plate to a white light source and comparing it with a plain acrylic plate, we realized that, first,

the formation of a hexagonal light pattern resulted in a clearer light contrast on the architected plate compared with the plain plate (Figure 5a). Second, thanks to a guided transmission of light through the prisms, the light intensity and shadow contrast were retained and transmitted, as evidenced by the preserved hexagonal pattern on the screen. In contrast, the light divergence amplified by the refraction of the plain plate did not allow a clear formation of the transmitted light spot, resulting in the blurring of the object's shadow.

Moreover, we hypothesized that the architectural organization of the prisms could lower the sensitivity to the incident angle of the light creating the image on the shell surface. Accordingly, we tested our hypothesis by exposing the plates to incident light at different angles (Figure S7a,b, Supporting Information). Remarkably, we found that the guided light transmission induced by the prismatic light guides can reduce, if not

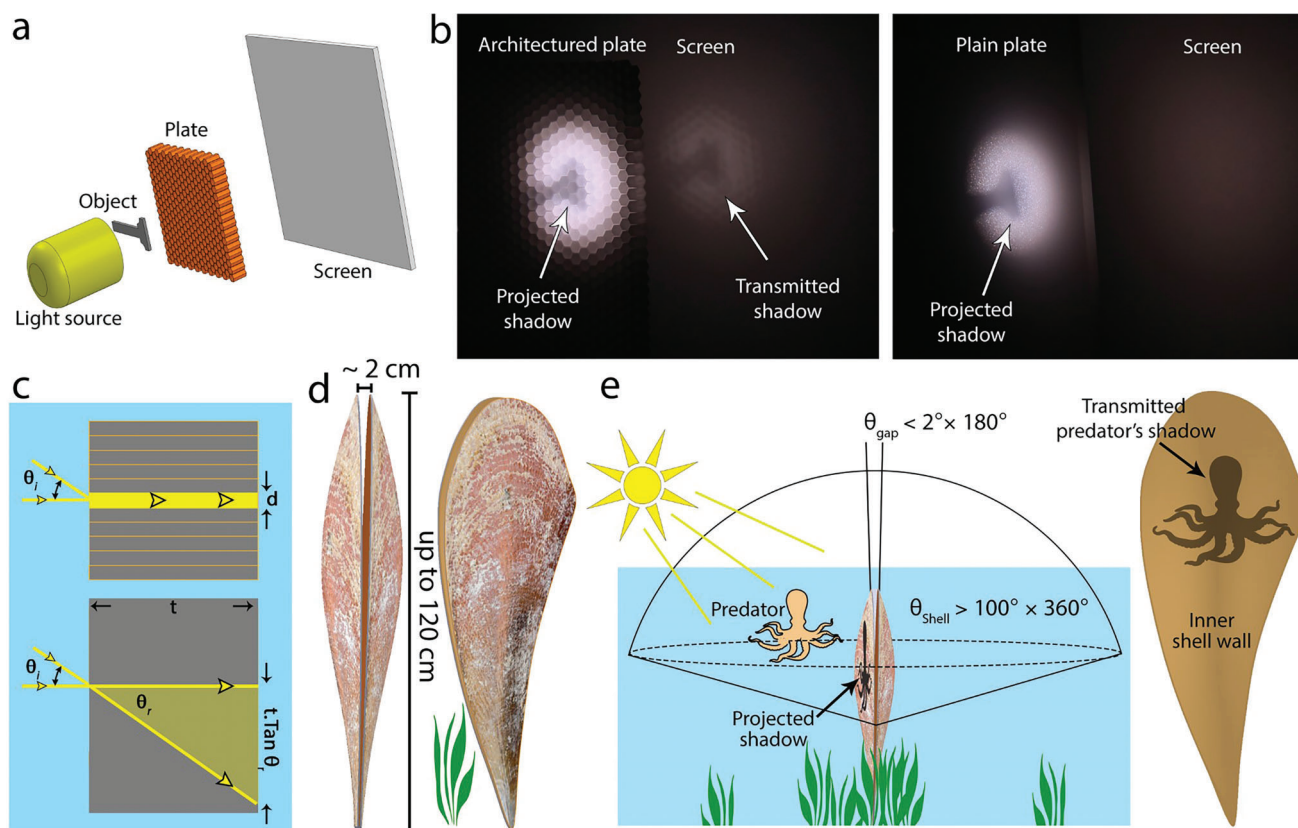


Figure 5. Shadow transmission through prismatic architecture. a) Schematic illustration of shadow projection setup used for studying the formation of reflected and transmitted shadows. b) Projected and transmitted lights on the architecture and plain acrylic plates. The prismatic light guides of the architected plate reduce the refraction drifts of the projected light spot on the screen resulting in the formation of a transmitted shadow on the screen. In contrast, the refraction in the plain panel prevents the formation of the transmitted shadow (Figure S7, Supporting Information). c) Schematic illustration presenting how the prismatic light guides promote a reduction in sensitivity to the incident angle, retain the incident light/projected shadow position, and result in the transmission of the shadow with high contrast and spatial resolution. d,e) Considering the narrow shell gap (minute light window), transmitting light/shadow through the prismatic layer can confer wide-angle light access on the animal independent of the sun/moon position. Note that despite the provided empirical evidence regarding the transfer of the projected shadow on the inner wall of the shell, it is not clear to what extent the animal can take advantage of such intricate optical characteristics. The illustration regarding the predator's shadows with a high spatial resolution does not imply that the animal can read the image.

cancel, the drifts in the position of the projected light spot, resulting in the reduction of the angular sensitivity for better spatial positioning of the light/shadow. In contrast, the transmitted light spot through a homogenous sample presented an obvious angular-dependent deviation from the incident point regulated by the RI and thickness of the plate (Figure 5c; Figure S7b,c, Supporting Information).

3. Conclusion

In summary, our observations provided empirical evidence of sophisticated light guide arrays integrated into the mechanical armors – shells – of *P. nobilis*, combining unlike and conflicting functions and forming a multifunctional structure.^[21d,26] We showed how the individual calcitic prisms act as optical fibers retaining and transferring the environmental light through total internal reflection to the inner shell cavity. We revealed that the bundled prisms – prismatic shell – form a light guide array converting the external light/shadow profile from a light intensity gradient to a pixelated intensity map and projecting it

on the inner shell surface. This conversion enhances the spatial resolution (defined by the prism diameter) and improves the contrast (achieved by sharp light intensity differences between neighboring prisms), yielding an optical feature suitable for the tracking of moving shadows. Notably, a similar pixel-array mechanism is being deployed in technological applications dedicated to image transferring^[27] or pre-processing spatial light information for advanced motion detection, edge-detection, and orientation-detection devices.^[28] This pre-processing implemented in the hardware through the pixel arrays reduces the complexity of the subsequent computational image processing.^[28c]

It is not clear, whether these exceptional optical characteristics of the *P. nobilis* prismatic shell correlate in any way with the animal's biological behavior. However, the reaction of *P. nobilis* to changes in environmental light intensity is documented,^[6b-d] and there are occasional reports that the animal closes its valves with a shadow approaching, which led to the suggestion that *P. nobilis* mantle possesses a light-sensing mechanism.^[6a] Indeed, the closure of the valves during the approach and the

presence of predators can be considered an essential precondition for effective protection. Considering the upright standing position of the animal (Figure S1, Supporting Information) and its limited gaping aperture (≈ 2 cm),^[6b,c] the shell gap only opens a narrow notch, which does not allow much access to surrounding light or shadows. In contrast, the translucency of the shell through the light guide arrays (prismatic bivalves) opens up a window with wide-angle visibility and significantly expands the animal's access to light and shadow of surrounding objects (Figure 5d,e). In addition to mechanical protection, light-sensing is known to play a role in the circadian clock of the animal.^[6d]

However, it remains to be proven that the revealed light guide array of the *P. nobilis* shell is part of a light-sensing or light-harvesting system to provide shadow tracking or imaging.^[23a,29] The detection of images by the animal would require an array of light sensors below the prismatic shell, for which there is currently no evidence. Nevertheless, a moving object's sharply structured spatial image generated by the light-guide array is converted to a sharply structured temporal sequence of light intensity (On–Off sequence, as shown in Figure 4) that may also be detected by a simple light-sensing system that does not provide any spatial resolution. We are also aware that invasive marine organisms, such as biofouling in the Mediterranean Sea, can influence these optical characteristics. However, we reason that considering the immense numbers of prisms (density of ≈ 500 prisms per inch, ppi), partial coverage of the shell by external objects does not block the access of the shell to the environmental light.

We propose that our findings may offer insights into the evolutionary aspects of light-sensing and imaging by biological materials and introduce a conceptual framework for the development of multifunctional transparent ceramics^[30] and architected light-tracking materials.

4. Experimental Section

Sample Collection: Two groups of *Pinna nobilis* and *Pinctada margaritifera* shells were used for the studies. The full-size shells were borrowed from the Naturkunde Museum of Berlin for photography, as depicted in Figure 1a–c). A series of wild smaller *P. nobilis* from the Mediterranean Sea and *Pinctada* from French Polynesia shells were used for material and optical studies.

Sample Preparation: Preparation of slices: To prepare the shell slides, *P. nobilis* shell pieces were directly polished using abrasive papers and colloidal particles down to $1\ \mu\text{m}$. For *Pinctada* samples, the nacreous and prismatic layers were first separated along the interfacial plane using a diamond wire saw ($d = 150\ \mu\text{m}$). Then, each layer was individually polished down to $1\ \mu\text{m}$. Preparation of individual prisms: Individual *P. nobilis* prisms were prepared by immersing small ($\approx 5\ \text{mm} \times 5\ \text{mm}$) shell pieces in a bleach solution (Solidum Hypochlorite) for 24 h at room temperature. Preparation of ODT sample: Individual *P. nobilis* prisms from the prismatic layer of the shell were fixed along the *c*-axis of calcite with DI water under $-20\ ^\circ\text{C}$ then cut into slices with a thickness of $\approx 30\ \mu\text{m}$ using a Leica Microtome (Leica CM3050 S, Leica Microsystems Nussloch GmbH, Germany). To separate the organic shields, small *P. nobilis* pieces were immersed for 48 h in a commercial acidic bleach solution (PH = 1.2, Ja Detergent Tab) at room temperature to bleach the calcitic prisms (Figure S8, Supporting Information). The bleached sample was rinsed and later sonicated in water for 5 min to separate the organic shields. Small droplets containing the organic shields were placed on the glass coverslips and were dried under

a fume hood. Preparation of polyacrylic samples: The architected replicated polyacrylic panels ($t = 2\ \text{mm}$) was designed and later outsourced for laser cutting. The pristine polyacrylic plates were used as a comparative reference.

Optical Microscopy: The optical images used in Figure 1b–e, Figure 5b,d, and Figure S2 (Supporting Information) were captured using a DSLR camera (EOS-500D, Canon) equipped with an EFS 18–200 lens (Canon). The optical micrograph of individual prisms (Figure 1g) was captured using a stereomicroscope (Leica-DVM6). Optical micrographs were captured using a microscope (Zeiss, AxioLab 5, Germany). For the studies in Figure 3b,c, an external light source (DH-2000-BAL, Ocean Insight), an optical fiber with a diameter of $200\ \mu\text{m}$, and a pinhole ($d = 10\ \mu\text{m}$, Thorlabs) were used to provide the transmission light. The sliced samples were placed directly on the top of the pinhole, and the transmitted light from the sample was collected using a $20\times$ objective lens (Zeiss).

Light Transmission and Reflection Studies: The light transmission and reflection studies were performed using a customized setup including a light source (DH-2000-BAL, Ocean Insight), a spectrometer (OCEAN-HDX-XR, Ocean Insight), and a set of optical cables (One Y-type fiber for reflection studies and two normal fibers for transmission studies). The collected spectra were extracted using OCEANVIEW (Ocean Insight) and then plotted by OriginPro 2020.

Ion-Sectioning: Ion-sectioning of the shell layer slices was done using a cross-section polisher (IB-19520CCP, JEOL) for 5 h of coarse cut (accelerating voltage 5.5 kV) followed by 1.5 h fine polishing (accelerating voltage 3 kV). To decrease/prevent the thermal damage to the organic residues, the sectioning was done in cryo-mode ($T = -120\ ^\circ\text{C}$), and a cutting cycle of 40 s On – 20 s Off was set for the cutting.

Electron Microscopy: Ion-sectioned samples were probed using a Field Emission Electron Microscope (FESEM, JEOL 7200) at an accelerating voltage of 5 kV. The samples were coated using carbon for $\approx 10\ \text{nm}$ prior to the study.

Light Interaction Studies on Individual Prisms: The studies on the individual *P. nobilis* prisms were performed under a stereomicroscope (Olympus, SZX7) equipped with an sCMOS camera (Andor, Zyla). The individual prism was inserted inside a pinhole ($d = 100\ \mu\text{m}$), and the gripped end was positioned in the rotation center of a swivel mount (Thorlabs). A spotlight using an optical fiber ($d = 200\ \mu\text{m}$) was exposed to the gripped end of the prism, and the transmitted light was captured from the free end of the prism at the incident angle of 0° , 10° , 20° , 30° , and 40° . The images were captured using the camera software (Andor Solis).

Shadow Projection: The transmission of projected shadow (Figure 5b) was investigated using a white light source (CoolLED, pE-4000) and a viewing screen (Thorlabs, EDU-VS1).

Optical Diffraction Tomography (ODT): The 3D RI of isolated calcitic prisms (thickness $20\text{--}30\ \mu\text{m}$) and unfolded organic shield layers (thickness $1\text{--}3\ \mu\text{m}$) was measured using a custom-built ODT microscope employing Mach–Zehnder interferometry similar to the one described in Ref. [18a]. The Mach–Zehnder interferometry measured spatially modulated holograms from 150 different angles, from which the complex optical fields were retrieved. The 3D RI tomograms were reconstructed by mapping 2D Fourier spectra of retrieved complex optical fields onto the surface of the Ewald sphere in the 3D Fourier space according to the Fourier diffraction theorem. Detailed principles for tomogram reconstruction can be found in Refs. [18b,c,31]. To image the prism and the organic layers, thin sections of each were sandwiched between two glass coverslips (VWR, Cat. No 631-0165). In order to reduce the RI mismatch between the samples and surrounding media, the prism layer was embedded in oil of $RI_{\text{oil}} = 1.6100$ (Series A Cargille Laboratories, Cat #: 1809), and the organic layer was embedded in oil of $RI_{\text{oil}} = 1.3950$ (Series AAA Cargille Laboratories, Cat #: 1803). The image acquisition, field retrieval, and RI tomogram reconstruction were performed using custom-written MATLAB scripts (R2020a). The mean RI value of each sample was measured with FIIJ^[32] and the statistical analysis was performed using GraphPad Prism.

Data Analysis: Data analysis and plotting were done using OriginPro software. Values were reported in mean \pm SD format.

Supporting Information

Supporting Information is available from the Wiley Online Library or from the author.

Acknowledgements

The authors thank J.P. Cuif for his generous help in providing the *Pinna nobilis* and *Pinctada margaritifera* shells samples and Jochen Guck for his support for RI mapping measurements. The authors thank Oliver Späker for his help with RI measurements. The authors acknowledge C. Zorn (Museum für Naturkunde, Berlin) for supporting by providing the *Pinna nobilis* and *Pinctada margaritifera* full-scale shells. The authors thank James C. Weaver for introducing the relative technological applications based on fiber optic bundles. The authors would also like to acknowledge Javier Murcia for generously providing the *P. nobilis* photograph (Figure 1a; Figure S1, Supporting Information) and use permissions. The project was funded by Max Planck Society. S.R. and A.B. acknowledge funding by the DFG (RE 3925/1-1) and Joachim Herz Stiftung, respectively.

Open access funding enabled and organized by Projekt DEAL.

Conflict of Interest

The authors declare no conflict of interest.

Author Contributions

S.A. and P.F. designed and developed the study. S.A., P.F., and M.A.C. designed the experiments. S.A. and T.Z. conducted the optical measurements. Y.D. provided the shell samples and insights regarding the studied models' biological characteristics. A.B., K.K., and S.R. conducted and analyzed the RI mapping studies. S.A. wrote the manuscript with input from all the authors.

Data Availability Statement

The data that support the findings of this study are available from the corresponding author upon reasonable request.

Keywords

architected materials, biological ceramics, functional ceramics, light guide arrays, light-tracking materials, materials multifunctionality, translucent ceramics

Received: May 4, 2023

Revised: July 7, 2023

Published online:

- [1] F. Barthelat, J. E. Rim, H. D. Espinosa, in *Applied Scanning Probe Methods XIII: Biomimetics and Industrial Applications*, (Eds: B. Bhushan, H. Fuchs), Springer, Berlin, Heidelberg **2009**.
- [2] A. G. Checa, *Front. Mar. Sci.* **2018**, *5*, 353.
- [3] J. D. C., *Proc. R. Soc. London, Ser. B* **1977**, *196*, 443.
- [4] O. B. Boggild, *Det Kongelige Danske Videnskaberne Selskabs Skrifter. Naturvidenskabelig og Matematisk Afdeling, Raekke* **1930**, *9*, 231.

- [5] a) Y. Dauphin, E. Zolotoyabko, A. Berner, E. Lakin, C. Rollion-Bard, J. P. Cuif, P. Fratzl, *J. Struct. Biol.* **2019**, *205*, 121; b) R. A. F. de Réaumur, **1717**.
- [6] a) G. Czihak, W. Dierl, *Pinna nobilis L.: eine Präparationsanleitung*, G. Fischer, Stuttgart **1961**; b) J. R. Garcia-March, S. Jiménez, M. A. Sanchis, S. Monleon, J. Lees, D. Surge, J. Tena-Medialdea, *Mar. Biol.* **2016**, *163*, 29; c) S. H. Caballero, J. R. G. March, M. Á. Sanchis, S. Monleón, N. Vicente, J. Tena, *Mediterr. Mar. Sci.* **2018**, *19*, 366; d) J. R. Garcia-March, M. Á. S. Solsona, A. M. García-Carrascosa, *Mar. Biol.* **2008**, *153*, 689.
- [7] D. Zavodnik, M. Hrs-Brenko, M. Legac, *Les espèces marines à protéger en Méditerranée* **1991**, 169.
- [8] C. A. Richardson, H. Kennedy, C. M. Duarte, D. P. Kennedy, S. V. Proud, *Mar. Biol.* **1999**, *133*, 205.
- [9] E. M. Harper, A. G. Checa, *Mar. Biol.* **2020**, *167*, 78.
- [10] L. Li, C. Ortiz, *Adv. Mater.* **2013**, *25*, 2344.
- [11] a) J. Bolman, *The mystery of the pearl*, Vol. 39, E. J. Brill, Leiden **1941**; b) F. Marin, P. Narayanappa, S. Motreuil, *Prog. Mol. Subcell. Biol.* **2011**, *52*, 353.
- [12] E. Hecht, *Optics*, Pearson, London **2012**.
- [13] J.-P. Cuif, Y. Dauphin, G. Luquet, K. Medjoubi, A. Somogyi, A. Perez-Huerta, *Minerals* **2018**, *8*, 370.
- [14] N. Watabe, K. Wada, *Rep. Fac. Fish., Prefect. Univ. Mie* **1956**, *2*, 227.
- [15] C. Lertvachirapaiboon, P. Pienpinijtham, K. Wongravee, S. Ekgasit, *ChemistrySelect* **2018**, *3*, 11700.
- [16] J. J. Wolken, *Light detectors, photoreceptors, and imaging systems in nature*, Oxford University Press, New York **1995**.
- [17] C. R. C. Sheppard, in *Beaches and Coastal Geology*, Springer US, New York, NY **1984**.
- [18] a) B. Abin, K. Kyoohyun, C. Gheorghe, G. Jochen, R. Simone, *Dev. Cell* **2021**, *56*, 967; b) E. Wolf, *Opt. Commun.* **1969**, *1*, 153; c) Y. Sung, W. Choi, C. Fang-Yen, K. Badizadegan, R. R. Dasari, M. S. Feld, *Opt. Express* **2009**, *17*, 266.
- [19] F. Marin, B. Pokroy, G. Luquet, P. Layrolle, K. D. Groot, *Biomaterials* **2007**, *28*, 2368.
- [20] R. W. Austin, G. Halikas, **1976**.
- [21] a) S. Johnsen, *Biol. Bull* **2001**, *201*, 301; b) G. Jacucci, L. Schertel, Y. Zhang, H. Yang, S. Vignolini, *Adv. Mater.* **2021**, *33*, 2001215; c) D. I. Speiser, D. J. Eernisse, S. Johnsen, *Curr. Biol.* **2011**, *21*, 665; d) L. Li, M. J. Connors, M. Kolle, G. T. England, D. I. Speiser, X. Xiao, J. Aizenberg, C. Ortiz, *Science* **2015**, *350*, 952.
- [22] B. Bayerlein, P. Zaslansky, Y. Dauphin, A. Rack, P. Fratzl, I. Zlotnikov, *Nat. Mater.* **2014**, *13*, 1102.
- [23] a) D.-E. Nilsson, in *Facets of Vision*, (Ed: R. C. H. Doekele, Ed: G. Stavenga), Springer, Berlin, Heidelberg, **1989**; b) E. Warrant, D.-E. Nilsson, *Invertebrate vision*, Cambridge University Press, Cambridge **2006**.
- [24] a) K. Franze, J. Grosche, S. N. Skatchkov, S. Schinkinger, C. Foja, D. Schild, O. Uckermann, K. Travis, A. Reichenbach, J. Guck, *Proc. Natl. Acad. Sci. U. S. A.* **2007**, *104*, 8287; b) J. Aizenberg, V. C. Sundar, A. D. Yablou, J. C. Weaver, G. Chen, *Proc. Natl. Acad. Sci. U. S. A.* **2004**, *101*, 3358; c) O. Spaeker, G. J. Taylor, B. D. Wilts, T. Slaby, M. A. K. Abdel-Rahman, E. Scoppola, C. N. Z. Schmitt, M. Sztucki, J. Liu, L. Bertinetti, W. Wagermaier, G. Scholtz, P. Fratzl, Y. Politi, *Adv. Sci.* **2022**, *9*, 2203371.
- [25] a) B. A. Palmer, A. Hirsch, V. Brumfeld, E. D. Afalo, I. Pinkas, A. Sagi, S. Rosenne, D. Oron, L. Leiserowitz, L. Kronik, S. Weiner, L. Addadi, *Proc. Natl. Acad. Sci. U. S. A.* **2018**, *115*, 2299; b) T. W. Cronin, *J. Crustacean Biol.* **1986**, *6*, 1.
- [26] M. Eder, S. Amini, P. Fratzl, *Science* **2018**, *362*, 543.
- [27] a) A. Orth, M. Ploschner, E. R. Wilson, I. S. Maksymov, B. C. Gibson, *Sci. Adv.* **2019**, *5*, eaav1555; b) M. Kyrish, R. Kester, R. Richards-Kortum, T. Tkaczyk, *Proc. SPIE Int. Soc. Opt. Eng.* **2010**, *7558*, 755807; c) T. Xie, D. Mukai, S. Guo, M. Brenner, Z. Chen, *Opt. Lett.* **2005**, *30*,

- 1803; d) A. Orth, M. Ploschner, I. S. Maksymov, B. C. Gibson, *Opt. Express* **2018**, 26, 6407.
- [28] a) S. Mashiyama, J. Hong, T. Ohtsuki, presented at *2015 IEEE International Conference on Communications (ICC)*, London, UK, June **2015**; b) G. Petrova, G. Spasov, I. Iliev, presented at *2021 XXX International Scientific Conference Electronics (ET)*, Sozopol, Bulgaria, September **2021**; c) N. D. Tam, *Adv. image video process.* **2014**, 2, 26.
- [29] D.-E. Nilsson, *Visual Neurosci.* **2013**, 30, 5.
- [30] a) T. Magrini, F. Bouville, A. Lauria, H. L.e Ferrand, T. P. Niebel, A. R. Studart, *Nat. Commun.* **2019**, 10, 2794; b) Z. Yin, F. Hannard, F. Barthelat, *Science* **2019**, 364, 1260.
- [31] K. Kim, H. Yoon, M. Diez-Silva, M. Dao, R. R. Dasari, Y. Park, *J. Biomed. Opt.* **2013**, 19, 011005.
- [32] J. Schindelin, I. Arganda-Carreras, E. Frise, V. Kaynig, M. Longair, T. Pietzsch, S. Preibisch, C. Rueden, S. Saalfeld, B. Schmid, *Nat. Methods* **2012**, 9, 676.